Phys. Proc. Ultra-Peripheral Collisions **2**, 013 (2026) 1-5

Onset of gluon saturation through incoherent J/ψ production at large $|t|$

A. Ridzikova[a], J. Cepila, J. G. Contreras, M. Matas
Faculty of Nuclear Sciences and Physical Engineering, Czech Technical University in Prague. Brehova 7, Prague, 112519 Czech Republic

In this contribution we predict the possibility of detecting signatures of the long-sought saturation in ultraperipheral heavy-ion collisions at currently accessible energies of the LHC. To probe these effects, we study incoherent vector meson production, which is sensitive to fluctuations in the partonic structure of the target. The energy-dependent hotspot model, formulated within the color dipole approach, incorporates subnucleonic degrees of freedom known as hotspots. Within this framework, we study the energy dependence of incoherent photoproduction of vector mesons in diffractive processes at various values of the Mandelstam-$|t|$ variable. Since $|t|$ is related to the transverse distribution of color charges, analyzing its energy dependence within specific ranges allows us to isolate fluctuations across different size scales, highlighting the hotspot contributions where saturation is expected.

DOI: https://doi.org/10.17161/5cpgd752
Keywords: parton saturation, vector meson production, hotspot model, incoherent process

1 Introduction

Understanding the internal structure of hadrons undergoing a hard interaction is one of the main directions of modern high-energy physics. In the small-x regime, parton densities grow rapidly, and perturbative QCD predicts that the gluon population eventually becomes large enough for recombination to counterbalance splitting, a phenomenon known as gluon saturation. Experimental insights into hadron structure were obtained from HERA measurements [1,2], are currently being pursued in ultraperipheral collisions at the LHC [3,4], and will be an important part of the physics program at future facilities such as the EIC [5].

A particularly efficient probe of this dense regime is the diffractive vector meson production, commonly studied within the color dipole picture [6,7]. Within this formalism, the scattering amplitude is governed by the interaction of a quark–antiquark dipole with the target, and thus depends directly on the color dipole cross section, which reflects the internal structure of the target. To capture this structure, geometric approaches that go beyond smooth density profiles are especially effective.

The energy-dependent hotspot model implements such an approach by representing the proton's transverse geometry through hotspots, fluctuating regions of high gluon density. Crucially, the number of hotspots increases with energy, enabling the model to reflect the evolving structure of the proton across energy scales while remaining computationally efficient. At low energies, corresponding to high values of x, the proton appears granular with only a few hotspots. As x decreases, the proton evolves into dense, homogeneous distribution, representing a proton completely filled with gluons. In this dense regime, the configurations become increasingly similar, which results in a reduction of the incoherent cross section. Early studies employing the model [8] predict that the incoherent J/ψ photoproduction cross section off protons rises with $W_{\gamma p}$, consistent with HERA measurements [9], and then decreases at higher energies, providing a signature of gluon saturation. We have extended these studies to nuclear targets, where saturation effects are expected to be stronger in heavy nuclei such as Pb and to appear at lower energies than in proton targets.

In this text, we explore the possibility of measuring saturation using the incoherent photoproduction of J/ψ as a function of both energy and $|t|$. Different ranges of $|t|$ probe structures of different spatial scales, where large $|t|$ values highlight contributions from subnucleonic fluctuations such as hotspots.

2 The hotspot model formalism

Coherent processes, in which the target remains intact, measure the overall geometry of the target, and therefore the cross section is calculated as an average of the scattering amplitude $\mathcal{A}_{\rm T,L}$ over all possible

[a]Speaker, email: ridziale@cvut.cz

configurations of the target H

$$\left.\frac{\mathrm{d}\sigma^{\gamma^*\mathrm{H}\to\mathrm{VH}}}{\mathrm{d}|t|}\right|_{\mathrm{T,L}} = \frac{\left(R_g^{\mathrm{T,L}}\right)^2}{16\pi}|\langle\mathcal{A}_{\mathrm{T,L}}\rangle|^2, \tag{1}$$

where indices T and L refer to transverse and longitudinal photon polarizations, respectively. The scattering amplitude reads [10]

$$\mathcal{A}_{\mathrm{T,L}}(x,Q^2,\vec{\Delta}) = i\int \mathrm{d}\vec{r}\int_0^1 \frac{\mathrm{d}z}{4\pi}\int \mathrm{d}\vec{b}|\Psi_{\mathrm{V}}^*\Psi_{\gamma^*}|_{\mathrm{T,L}}\exp\left[-i\left(\vec{b}-\left(\frac{1}{2}-z\right)\vec{r}\right)\vec{\Delta}\right]\frac{\mathrm{d}\sigma_{\mathrm{H}}^{\mathrm{dip}}}{\mathrm{d}\vec{b}}, \tag{2}$$

where the factor $|\Psi_{\mathrm{V}}^*\Psi_{\gamma^*}|_{\mathrm{T,L}}$ represents the overlap between the photon wave function, which describes the splitting of the photon into a dipole, and the model-dependent vector meson wave function, for which we use boosted Gaussian model [11,12,13] with parameters taken from [14]. The vector $\vec{b}$ represents the impact parameter, $\vec{r}$ denotes the transverse separation of the quark–antiquark dipole, and z is the fraction of the photon momentum carried by quark. Here, x is the Bjorken variable, which in this case takes the form

$$x = \frac{Q^2+M_V^2}{Q^2+W^2}, \tag{3}$$

where Q^2 is the photon virtuality, M_V is the mass of produced vector meson and W is center-of-mass energy of the photon–target system. The vector $\vec{\Delta}$ is momentum transferred in the interaction, related to the Mandelstam variable by $\vec{\Delta}^2 \equiv -t$.

In contrast, incoherent processes, in which the target breaks up, are sensitive to event-by-event fluctuations, and the corresponding cross section is proportional to the variance of the scattering amplitude over target configurations,

$$\left.\frac{\mathrm{d}\sigma^{\gamma^* H\to\mathrm{V}Y}}{\mathrm{d}|t|}\right|_{\mathrm{T,L}} = \frac{\left(R_g^{T,L}\right)^2}{16\pi}\left(\langle|\mathcal{A}_{\mathrm{T,L}}|^2\rangle - |\langle\mathcal{A}_{\mathrm{T,L}}\rangle|^2\right). \tag{4}$$

The factor $R_g^{\mathrm{T,L}}$ accounts for the skewedness correction [15],

$$R_g^{\mathrm{T,L}} = \frac{2^{2\lambda_g^{\mathrm{T,L}}+3}}{\sqrt{\pi}}\frac{\Gamma(\lambda_g^{\mathrm{T,L}}+5/2)}{\Gamma(\lambda_g^{\mathrm{T,L}}+4)}, \qquad \lambda_g^{\mathrm{T,L}} \equiv \frac{\partial\ln(A_{\mathrm{T,L}})}{\partial\ln(1/x)}, \tag{5}$$

calculated at $t=0$.

The cross section for a color dipole scattering off a proton is given by

$$\frac{\mathrm{d}\sigma_{\mathrm{p}}^{\mathrm{dip}}}{\mathrm{d}\vec{b}} = \sigma_0 N(x,r)T_{\mathrm{p}}(\vec{b}), \tag{6}$$

where we use the GBW [16] model to calculate the scattering amplitude.

The proton profile is determined by the sum of the individual hotspot profiles over the total number of hotspots. The positions of hotspots are randomly sampled from a 2D Gaussian distribution, and each hotspot has a Gaussian distribution,

$$T_{\mathrm{p}}(\vec{b}) = \frac{1}{N_{\mathrm{hs}}}\sum_{i=1}^{N_{\mathrm{hs}}} T_{\mathrm{hs}}\left(\vec{b}-\vec{b}_i\right), \tag{7}$$

$$T_{\mathrm{hs}}\left(\vec{b}-\vec{b}_i\right) = \frac{1}{2\pi B_{\mathrm{hs}}}\exp\left(-\frac{\left(\vec{b}-\vec{b}_i\right)^2}{2B_{\mathrm{hs}}}\right). \tag{8}$$

The dipole proton cross section can be extended to the dipole nucleus cross section by employing the Glauber model with Gribov corrections [17], which reads

$$\left(\frac{\mathrm{d}\sigma_{\mathrm{A}}^{\mathrm{dip}}}{\mathrm{d}\vec{b}}\right) = 2\left[1-\left(1-\frac{1}{2A}\sigma_0 N(x,r)T_{\mathrm{A}}(\vec{b})\right)^A\right]. \tag{9}$$

Within the hotspot model, the nuclear profile is defined as

$$T_{\rm hs}(\vec{b}-\vec{b}_i) = \frac{1}{2\pi B_{\rm hs}} \sum_{i=1}^{A=208} \frac{1}{N_{\rm hs}} \sum_{j=1}^{N_{\rm hs}} \exp\left(-\frac{\left(\vec{b}-\vec{b}_i-\vec{b}_j\right)^2}{2B_{\rm hs}}\right), \tag{10}$$

where $\vec{b}_i$ denotes the transverse position of the i-th nucleon in the nucleus and $\vec{b}_j$ specifies the location of a hotspot within that nucleon. The parameter $B_{\rm hs}$ controls the transverse size of each hotspot. For lead nuclei, the nucleon positions are distributed according to a Woods–Saxon profile.

The strength of this model is that it introduces an indirect energy dependence into the proton profile by allowing the number of hotspots, $N_{\rm hs}(x)$, to increase as x decreases. The value of $N_{\rm hs}$ is sampled from a zero-truncated Poisson distribution, with the underlying Poisson distribution characterized by a mean value [8,18]:

$$\langle N_{hs}(x)\rangle = p_0 x^{p_1}(1+p_2\sqrt{x}). \tag{11}$$

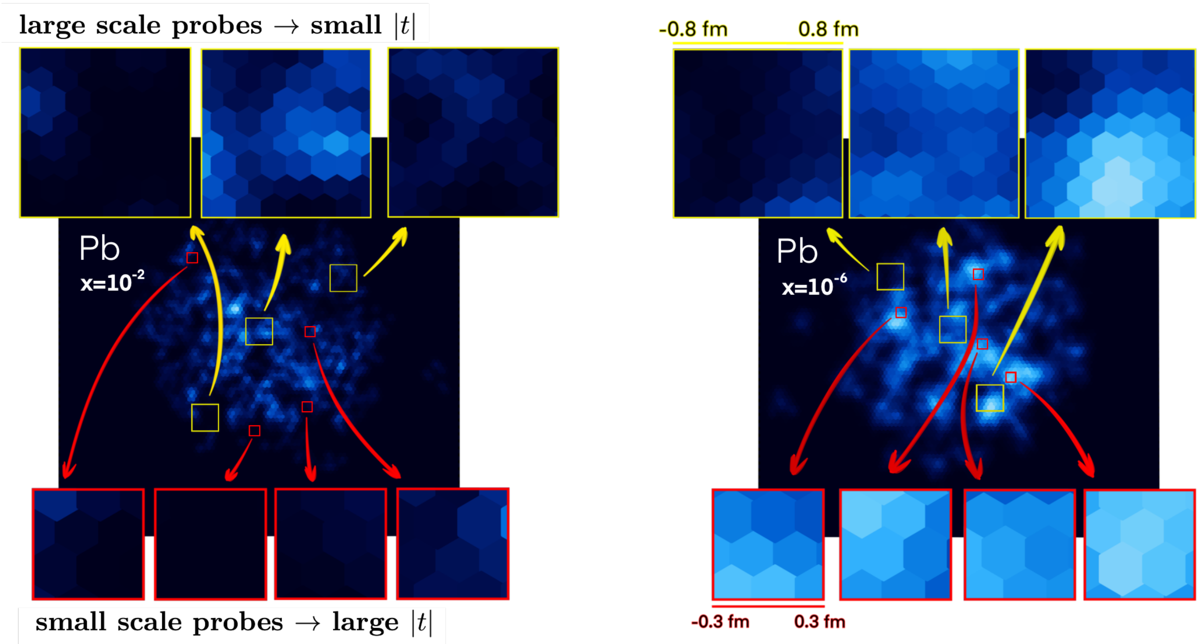

Figure 1 – The structure of lead generated using the energy-dependent hotspot model for Bjorken-x=10^{-2} (left) and x=10^{-6} (right). The yellow boxes represent large-scale probes of size $\sim$ 0.8 fm, corresponding to small $|t|$. At this scale, noticeable variance is observed both at low and high energies, leading to an increase of the cross section at small values of $|t|$ with energy. In contrast, the red boxes denote small-scale probes of size $\sim$ 0.3 fm, corresponding to large-$|t|$ sensitivity to hotspot sizes. At large x, these regions are often nearly empty, leading to minimal variance and thus a suppressed incoherent cross section. At small x, the regions are densely populated with hotspots which therefore again causes limited variance. As a result, the incoherent cross section at large $|t|$ first increases with energy as the number of hotspots grows, reaches a maximum, and then decreases once the hotspot density becomes too large.

3 Results

Using the energy-dependent hotspot model, we compute the cross section for the coherent and incoherent photoproduction of the J/ψ vector meson off the lead target. Figure 2 presents the Mandelstam-$|t|$ dependence. A comparison with ALICE data [19,20] indicates that our model describes correctly the incoherent production within the current experimental uncertainties but overestimates the coherent contribution.

Figure 3 suggests a new way to identify saturation at the LHC: the incoherent photoproduction of J/ψ in diffractive γPb interactions as a function of energy at fixed values of $|t|$. For small $|t|$, the cross section follows a power-law growth with energy. A similar increase is observed for intermediate values, $|t| = 0.1$ GeV^2 and $|t| = 0.5$ GeV^2. At large $|t| = 1$ GeV^2, where the contribution of hotspots dominate, the behavior changes: the cross section rises with energy, reaches a maximum and then decreases. This turnover signals the onset of saturation. Recently, the ALICE Collaboration [21] measured the energy dependence of incoherent J/ψ photoproduction off lead in three $|t|$ intervals, from 0.09 to 1.44 GeV^2. Their results reveal that, at large $|t|$, the increase of the cross section with energy is suppressed compared to the rise seen at small $|t|$, which is in qualitative agreement with the expectations of our model. However, the position of the maximum in the J/ψ cross section has not yet been observed, and it seems to lay at energies just beyond those covered by the currently available data.

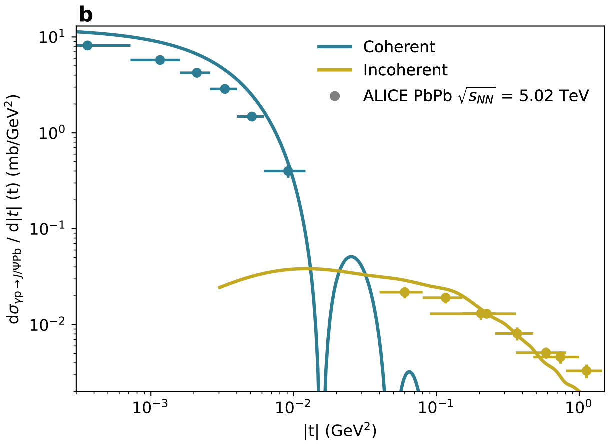

Figure 2 – Mandelstam-$|t|$ dependence of J/ψ photoproduction off Pb at an energy W= 125 GeV. The markers show data from the ALICE [19,20] collaboration, while the lines depict the predictions of our model. Figure taken from [22].

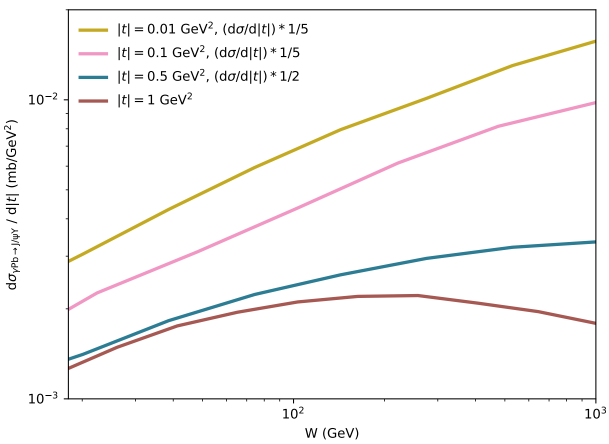

Figure 3 – Predictions of the energy-dependent hotspot model for the incoherent J/ψ photoproduction at fixed $|t|$ in γPb diffractive interactions. Some of the lines have been scaled to improve readability of the figure. Figure taken from [22].

4 Summary

In this report, we presented predictions from the energy-dependent hotspot model, focusing on the possible onset of gluon saturation in ultraperipheral Pb–Pb collisions at the LHC.

Our results indicate that gluon saturation could be observed through incoherent J/ψ photoproduction at large $|t|$, where the contributions of hotspots are most relevant. At these large values of $|t|$, the incoherent cross section is predicted to reach a maximum, marking the onset of saturation. Current ALICE measurements show a plateau in the energy dependence of the cross section at large $|t|$, although the actual turnover may lie beyond the reach of the data and the forthcoming data on both ρ^0 and J/ψ photoproduction will provide further insight.

References

1. Paul Newman and Matthew Wing. The Hadronic Final State at HERA. *Rev. Mod. Phys.*, 86(3):1037, 2014.
2. H. Abramowicz et al. Combination of measurements of inclusive deep inelastic $e^{\pm}p$ scattering cross sections and QCD analysis of HERA data. *Eur. Phys. J. C*, 75(12):580, 2015.
3. J. G. Contreras and J. D. Tapia Takaki. Ultra-peripheral heavy-ion collisions at the LHC. *Int. J. Mod. Phys. A*, 30:1542012, 2015.
4. A. J. Baltz et al. The Physics of Ultraperipheral Collisions at the LHC. *Phys. Rept.*, 458:1–171, 2008.
5. A. Accardi et al. Electron Ion Collider: The Next QCD Frontier: Understanding the glue that binds us all. *Eur. Phys. J. A*, 52(9):268, 2016.
6. Alfred H. Mueller. Small x Behavior and Parton Saturation: A QCD Model. *Nucl. Phys. B*, 335:115–137, 1990.
7. Alfred H. Mueller and Bimal Patel. Single and double BFKL pomeron exchange and a dipole picture of high-energy hard processes. *Nucl. Phys. B*, 425:471–488, 1994.
8. J. Cepila, J. G. Contreras, and J. D. Tapia Takaki. Energy dependence of dissociative J/ψ photoproduction as a signature of gluon saturation at the LHC. *Phys. Lett.*, B766:186–191, 2017.
9. C. Alexa et al. Elastic and Proton-Dissociative Photoproduction of J/psi Mesons at HERA. *Eur. Phys. J. C*, 73(6):2466, 2013.
10. H. Kowalski, L. Motyka, and G. Watt. Exclusive diffractive processes at HERA within the dipole picture. *Phys. Rev.*, D74:074016, 2006.
11. J. Nemchik, Nikolai N. Nikolaev, and B. G. Zakharov. Scanning the BFKL pomeron in elastic production of vector mesons at HERA. *Phys. Lett. B*, 341:228–237, 1994.
12. J. Nemchik, Nikolai N. Nikolaev, E. Predazzi, and B. G. Zakharov. Color dipole phenomenology of diffractive electroproduction of light vector mesons at HERA. *Z. Phys. C*, 75:71–87, 1997.
13. Jeffrey R. Forshaw, R. Sandapen, and Graham Shaw. Color dipoles and rho, phi electroproduction. *Phys. Rev. D*, 69:094013, 2004.
14. D. Bendova, J. Cepila, and J. G. Contreras. Dissociative production of vector mesons at electron-ion colliders. *Phys. Rev. D*, 99(3):034025, 2019.
15. A. G. Shuvaev, Krzysztof J. Golec-Biernat, Alan D. Martin, and M. G. Ryskin. Off diagonal distributions fixed by diagonal partons at small x and xi. *Phys. Rev. D*, 60:014015, 1999.
16. Krzysztof J. Golec-Biernat and M. Wusthoff. Saturation effects in deep inelastic scattering at low Q**2 and its implications on diffraction. *Phys. Rev. D*, 59:014017, 1998.
17. N. Armesto. A Simple model for nuclear structure functions at small x in the dipole picture. *Eur. Phys. J. C*, 26:35–43, 2002.
18. Jan Cepila, Jesus Guillermo Contreras, and Michal Krelina. Coherent and incoherent J/ψ photonuclear production in an energy-dependent hot-spot model. *Phys. Rev. C*, 97(2):024901, 2018.
19. Shreyasi Acharya et al. First measurement of the —t—-dependence of coherent J/ψ photonuclear production. *Phys. Lett. B*, 817:136280, 2021.
20. Shreyasi Acharya et al. First Measurement of the —t— Dependence of Incoherent J/ψ Photonuclear Production. *Phys. Rev. Lett.*, 132(16):162302, 2024.
21. Shreyasi Acharya et al. Evidence for J/ψ suppression in incoherent photonuclear production. 3 2025.
22. Jan Cepila, Jesus Guillermo Contreras, Marek Matas, and Alexandra Ridzikova. Incoherent J/ψ production at large $|t|$ identifies the onset of saturation at the LHC. *Phys. Lett. B*, 852:138613, 2024.